Nonlinear theory of free-electron lasers and efficiency enhancement

P. Sprangle, Cha-Mei Tang,* and W. M. Manheimer

Naval Research Laboratory, Washington, D. C. 20375

(Received 16 July 1979)

The development of lasers in which the active medium is a relativistic stream of free electrons has recently evoked much interest. The potential advantages of such free-electron lasers include, among other things, continuous frequency tunability, very high operating power, and high efficiency. The free-electron laser (FEL) is characterized by a pump field, for example, a spatially periodic magnetic field which scatters from a relativistic-electron beam. The scattered radiation has a wavelength much smaller than the pump wavelength, depending on the electron-beam energy. The authors present a general self-consistent nonlinear theory of the FEL process. The nonlinear formulation of the temporal steady-state FEL problem results in a set of coupled differential equations governing the spatial evolution of the amplitudes and wavelength of the radiation and space-charge fields. These equations are readily solved numerically since the amplitude and wavelength vary on a spatial scale which is comparable to a growth length of the output radiation. A number of numerical and analytical illustrations are presented, ranging from the optical to the submillimeter-wavelength regime. Our nonlinear formulation in the linear regime is compared with linear theory, and agreement is found to be excellent. Analytical expressions for the saturated efficiency and radiation amplitude are also shown to be in very good agreement with our nonlinear numerical solutions. Efficiency curves are obtained for both the optical and submillimeter FEL examples with fixed magnetic-pump parameters. It is shown that these intrinsic efficiencies can be greatly enhanced by appropriately contouring the magnetic-pump period. In the case of the optical FEL, the theoretical single-pass efficiency can be made greater than 20% by appropriately decreasing the pump period and increasing the pump magnetic field.

I. INTRODUCTION

Free-electron lasers (FEL's) based on backscattering from relativistic electron beams have demonstrated a unique potential for becoming a new type of coherent radiation source. In principle, these radiation sources will be characterized by output wavelengths ranging from the millimeter to beyond the optical regime, frequency tunability, very high power levels, and high efficiencies.

Theoretical analysis on the FEL mechanism has been carried out in the single-particle[1-18] as well as the collective scattering regime.[7,11,15,17-26] Also, nonlinear processes and saturation efficiencies have been considered for various FEL scattering regimes.[6,8,15,17,18,23,24,27]

The operative mechanism in FEL's is a parametric process in which a long-wavelength pump field interacts with a beam of relativistic electrons. Under certain conditions the incident pump field will decay into a longitudinal wave (density wave) and a backscattered electromagnetic wave which is double Doppler upshifted in frequency. The longitudinal wave (also referred to as density wave, beat wave, or ponderomotive wave) results from the coupling of the pump field and the electromagnetic field through the $\vec{v} \times \vec{B}/c$ force term. The ponderomotive wave plays a central role in the linear and nonlinear development of the scattering process. Its effect on the electron beam is closely analogous to the role played by the negative-energy (slow-space-charge) wave in conventional traveling-wave mechanisms.

The pump field may take the form of a static spatially periodic magnetic or electric field or a propagating electromagnetic wave. In this paper we take the pump to be a static, periodic, right-handed, helically polarized, magnetic field. The frequency of the scattered radiation is given by

$$\omega \approx (1 + v_z/c)\gamma_z^2 v_z (2\pi/l) \approx 4\pi\gamma_z^2 c/l,$$

where

$$\gamma_z = (1 - v_z^2/c^2)^{-1/2},$$

v_z is the axial beam velocity, and l is the pump period. The possibility of using a two-stage FEL scattering process, in order to reduce the electron energy required for very short output wavelengths, has been suggested.[14,18]

Roughly speaking, FEL's can be divided into two categories, depending on the gain of the radiation field. In the low-gain regime, the overall spatially integrated gain is due to wave interference effects and is much less than unity. This is a single-particle (collective effects are not manifested through space-charge fields) scattering regime and is exemplified by experiments at Stanford University.[28,29]

The high-gain FEL's are characterized by stimulated radiation fields which grow exponentially in the linear regime. Experiments with intense relativistic electron beams performed at Naval Research Laboratory (NRL), Columbia University, and Cornell University fall into this class.[30-35]

For a detailed theoretical discussion of the various FEL mechanisms the reader is referred to Refs. 11, 17, and 18.

The main objectives of this work are to present a self-consistent nonlinear formulation of the FEL mechanism and to theoretically analyze some of the concepts necessary to develop efficient, high-power, tunable FEL radiation sources. Some of the salient features of this theory include: (i) completely arbitrary magnetic-pump field (period and amplitude can be functions of axial position) (ii) space-charge effects, (iii) arbitrary polarization of the radiation field, (iv) completely relativistic particle dynamics, and (v) frequency and spatial harmonics in the excited fields. The nonlinear formalism developed for the FEL problem is also applicable to a large class of temporal steady-state convective processes. Our formulation of the problem permits the spatial dependence of the pump magnetic field to be arbitrary. Hence efficiency enhancement schemes which utilize amplitude and wavelength spatial variations of the pump field can be analyzed. The spatial variation of the scattered-radiation amplitude and wavelength occurs on a scale-length which is large compared to the wavelength of the pump field. This permits numerical solutions for cases where the electron-beam energy is extremely high. That is, in this approach, there is no large separation of spatial-scale lengths, despite the large spatial-scale difference between the wavelength of the scattered field and the pump field; so arbitrarily high values of the relativistic gamma factor γ associated with the beam, can be considered. Furthermore, the formulation is carried out in the laboratory frame under temporal steady-state conditions.

The analytical formulation of the general nonlinear steady-state FEL problem consists essentially of three parts. In Sec. II, the wave equations are used to derive expressions for the slow spatial evolution of the amplitudes and phases of the scattered fields in terms of the driving currents. Then, in Sec. III, the driving currents are expressed as functions of the dynamics of the particle ensemble (electron-distribution function). The particle orbit equations are written self-consistently in terms of the scattered fields in Sec. IV. The orbit equations describing the motion transverse and parallel to the electron stream are completely decoupled. The linear spatial growth rates, efficiencies, and saturated-field amplitudes are derived in Sec. V for various scattering regimes. Finally, a number of analytical–numerical illustrations in the high-gain scattering regime are then given in Sec. VI. The nonlinear particle dynamics is discussed in some detail. Efficiency curves are obtained, and a method of dramatically increasing the single-pass efficiency, as suggested in Ref. 17, by contouring both the pump period and magnetic field, is analyzed.[36] For instance, efficiencies of >20% are shown to be theoretically possible at optical wavelengths using this approach. The basic idea is to gradually slow down the phase velocity of the ponderomotive wave at the point where the electrons are deeply trapped in the ponderomotive wave potentials. The slowing down of the wave is accomplished by adiabatically decreasing the pump field period. The appendix contains the formulation of the FEL process with spatial and temporal harmonics in both the radiation and space-charge fields. Also included in this formulation is the ability of the radiation field to undergo a change in polarization from a circularly polarized to an ellipically polarized wave as the particle dynamics become nonlinear.

The resulting set of nonlinear coupled equations self-consistently relate the spatial dynamics of the particles and fields. These equations have been solved analytically in the linear approximation and the linear dispersion relation has been obtained. The full set of nonlinear coupled equations are readily solved numerically for the spatial growth rate and saturation level of the scattered fields.

II. NONLINEAR EVOLUTION OF SCATTERED WAVES

The physical model we will develop is that of a fully relativistic electron beam interacting with a spatially periodic pump magnetic field as depicted in Fig. 1. Only spatial variations along the z axis will be considered for the electron beam, pump field, and scattered-radiation field.

The variable amplitude and period pump magnetic field can be expressed in terms of the vector potential

$$\vec{A}_0(z) = A_0(z) \left[\cos\left(\int_0^z k_0(z')dz' \right) \hat{e}_x \right.$$
$$\left. + \sin\left(\int_0^z k_0(z')dz' \right) \hat{e}_y \right], \qquad (1)$$

where the amplitude $A_0(z)$ and wave number $k_0(z)$ are known and are slowly varying functions of z. The potential field in Eq. (1) is a good approximation of a right-handed polarized helical magnetic field near the z axis of an appropriate coil winding. The pump magnetic field associated with Eq. (1) is given by

$$\vec{B}_0(z) = B_0(z) \left[\cos\left(\int_0^z k_0(z')dz' + \varphi(z) \right) \hat{e}_x \right.$$
$$\left. + \sin\left(\int_0^z k_0(z')dz' + \varphi(z) \right) \hat{e}_y \right], \qquad (2)$$

FEL CONFIGURATION

E.M. AND E.S. FIELDS, $\underset{\sim}{A}(z,t)$, $\phi(z,t)$

MAGNETIC PUMP
FIELD $\underset{\sim}{A}_0(z)$ |—— l ——|

|———————— INTERACTION REGION ————————|
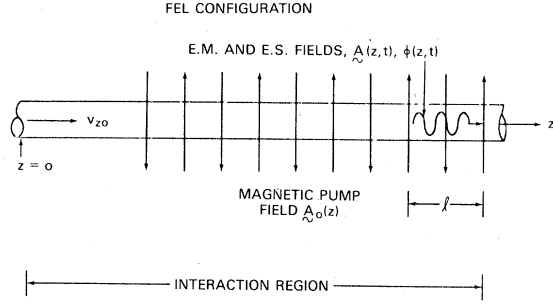
FIG. 1. Schematic of the free-electron-laser model. The unmodulated electron beam enters the interaction region from the left. In this figure the pump field builds up adiabatically and reaches a constant amplitude and wavelength for $z > 0$. The pump field may in general have a varying period and amplitude, which is not shown in the figure.

where

$$B_0(z) = -\left[[k_0(z)A_0(z)]^2 + \left(\frac{\partial A_0(z)}{\partial z^2}\right)^2 \right]^{1/2}$$

and

$$\varphi(z) = -\tan^{-1}\frac{\partial A_0(z)/\partial z}{k_0(z)A_0(z)}$$

are slowly varying functions of z. The period of the magnetic field is

$$l(z) = 2\pi/[k_0(z) + \partial\varphi/\partial z] \approx 2\pi/k_0(z) . \tag{3}$$

The scattered electromagnetic and electrostatic fields in terms of the vector potential $\vec{A}(z,t)$ and scalar potential $\phi(z,t)$ are taken to be

$$\vec{A}(z,t) = A_x(z)\cos\left(\int_0^z k_+(z')dz' - \omega t + \theta \right)\hat{e}_x$$

$$- A_y(z)\sin\left(\int_0^z k_+(z')dz' - \omega t + \theta \right)\hat{e}_y ,$$

$$\tag{4a}$$

$$\phi(z,t) = \phi(z)\cos\left(\int_0^z k(z')dz' - \omega t + \theta_z \right), \tag{4b}$$

where the amplitudes of the potentials $A_x(z)$, $A_y(z)$, and $\phi(z)$ as well as the wave numbers $k_+(z)$ and $k(z)$ are slowly varying functions of z. The scattered electromagnetic field represented by Eq. (4a) is a right-handed elliptically polarized field traveling towards the right. The frequency ω of the field and the phases θ and θ_z are independent of z. In the appendix, the general form for the scattered fields is used in the nonlinear formulation of the problem. However, in the main body of the text, the fields in Eqs. (4) will be used in order to minimize the notational algebra.

The evolution of the scattered potentials is governed by the wave equations

$$\left(\frac{\partial^2}{\partial z^2} - \frac{1}{c^2}\frac{\partial^2}{\partial t^2}\right)\vec{A}(z,t) = -\frac{4\pi}{c}\vec{J}_\perp(z,t) , \tag{5a}$$

and

$$\frac{\partial^2\phi(z,t)}{\partial z\,\partial t} = 4\pi J_z(z,t) , \tag{5b}$$

where $\vec{J}(z,t)$ is the driving current density. Substituting the potentials of Eqs. (4) into (5), we obtain

$$[\omega^2/c^2 - k_+^2(z)]A_x(z)\cos\psi(z,t)$$

$$-2k_+^{1/2}(z)\frac{\partial}{\partial z}[A_x(z)k_+^{1/2}(z)]\sin\psi(z,t)$$

$$= -\frac{4\pi}{c}J_x(z,t) , \tag{6a}$$

$$[\omega^2/c^2 - k_+^2(z)]A_y(z)\sin\psi(z,t)$$

$$+2k_+^{1/2}\frac{\partial}{\partial z}[A_y(z)k_+^{1/2}(z)]\cos\psi(z,t) = \frac{4\pi}{c}J_y(z,t) , \tag{6b}$$

$$\frac{\partial\phi(z)}{\partial z}\sin\psi_z(z,t) + k(z)\phi(z)\cos\psi_z(z,t)$$

$$= \frac{4\pi}{\omega}J_z(z,t) , \tag{6c}$$

where

$$\psi(z,t) = \int_0^z k_+(z')dz' - \omega t + \theta ,$$

with

$$\psi_z(z,t) = \int_0^z k(z')dz' - \omega t + \theta_z .$$

Terms proportional to $\partial^2 A/\partial z^2$ have been neglected from Eqs. (6). The neglect of $\partial^2 A/\partial z^2$ terms is not central to our formulation, though it can be shown to be an excellent approximation which simplifies the final FEL equations. The coefficients of the sinusoidal terms on the left-hand side of Eqs. (6) are slowly varying functions of z and independent of t. The arguments of the sinusoidal terms, on the other hand, are rapidly varying functions of t for fixed z. The rapidly time-varying terms in, for example, Eq. (6a) can be removed by multiplying it by cos (or sin) $\psi(z,t)$ and taking the temporal average over one wave period, i.e., $(\omega/2\pi)\int_0^{2\pi/\omega}dt$. Performing this operation on Eq. (6a) as well as similar ones on Eqs. (6b) and (6c), we obtain

$$[\omega^2/c^2 - k_+^2(z)]A_x(z)$$

$$= \frac{-4\omega}{c}\int_0^{2\pi/\omega}J_x(z,t)\cos\psi(z,t)dt , \tag{7a}$$

$$2k_+^{1/2}(z)\frac{\partial}{\partial z}[A_x(z)k_+^{1/2}(z)]$$

$$=\frac{4\omega}{c}\int_0^{2\pi/\omega} J_x(z,t)\sin\psi(z,t)dt, \quad (7b)$$

$$[\omega^2/c^2 - k_+^2(z)]A_y(z)$$

$$=\frac{4\omega}{c}\int_0^{2\pi/\omega} J_y(z,t)\sin\psi(z,t)dt, \quad (7c)$$

$$2k_+^{1/2}(z)\frac{\partial}{\partial z}[A_y(z)k_+^{1/2}(z)]$$

$$=\frac{4\omega}{c}\int_0^{2\pi/\omega} J_y(z,t)\cos\psi(z,t)dt, \quad (7d)$$

$$\frac{\partial\phi(z)}{\partial z}=4\int_0^{2\pi/\omega} J_z(z,t)\sin\psi_z(z,t)dt, \quad (7e)$$

$$k(z)\phi(z)=4\int_0^{2\pi/\omega} J_z(z,t)\cos\psi_z(z,t)dt. \quad (7f)$$

III. DERIVATION OF NONLINEAR DRIVING CURRENTS

It is now necessary to derive expressions for the x, y, and z components of the current densities and perform the time integration specified in Eqs. (7). In general the nonthermal electron distribution function, written in terms of the electron orbits, is

$$f(z,\vec{p},t)=n_0\nu_{z0}\int_{-\infty}^{\infty} \delta(z - \xi(t_0,t))\delta(p_x - \eta_x(t_0,t))$$

$$\times\,\delta(p_y - \eta_y(t_0,t))\delta(p_z - \eta_z(t_0,t))dt_0$$

$$(8)$$

where n_0 is the uniform particle density to the left of the interaction region, i.e., $z \le 0$, ν_{z0} is the constant axial electron velocity for $z \le 0$, $\xi(t_0,t)$ is the axial position of the particle at time t which crossed the $z = 0$ plane at time t_0, and $\vec{\eta}(t_0,t)$ is the momentum vector of the particle at time t which crossed the $z = 0$ plane at time t_0. Thermal effects which are characteristic of actual electron beams can be easily included by appropriately modifying the electron distribution function in Eq. (8). The integral over t_0 in Eq. (8) takes into account the continuous flow of particles into the interaction region. The current density associated with this electron distribution is

$$\vec{J}(z,t)=-|e|\int \frac{\vec{p}}{\gamma(\vec{p})m_0}f(z,\vec{p},t)d\vec{p}$$

$$=\frac{-|e|n_0\nu_{z0}}{m_0}\int_{-\infty}^{\infty} \frac{\vec{\eta}(t_0,t)}{\gamma(\vec{\eta}(t_0,t))}\,\delta(z - \xi(t_0,t))dt_0,$$

$$(9)$$

where $\gamma(\vec{\eta}) = (1 +\vec{\eta}^2/m_0^2c^2)^{1/2}$. As will be seen later

it is necessary to rewrite Eq. (9) in the form

$$\vec{J}(z,t)=\frac{-|e|n_0\nu_{z0}}{m_0}$$

$$\times\int_{-\infty}^{\infty} \frac{\vec{\eta}(t_0,t)\delta(t - \tau(t_0,z))}{\gamma(\vec{\eta}(t_0,t))|\partial\xi(t_0,t)/\partial t|}\,dt_0, \quad (10)$$

where

$$\tau(t_0,z)=t_0+\int_0^z \frac{dz'}{\nu_z(t_0,z')} \quad (11)$$

is the time it takes a particle to reach the position z if it entered the interaction region $z = 0$ at time t_0 and $\nu_z(t_0,z)$ is the axial velocity of a particle at position z which was at $z = 0$ at time t_0.

The quantity $\partial\xi(t_0,t)/\partial t$ is the axial velocity ν_z of a particle at time t which was at $z = 0$ at time t_0. Clearly, for $\vec{J}(z,t)$ to be finite, ν_z should not vanish in the interaction region. If ν_z vanishes and particles are turned around, multistreaming develops and the entire concept of $\exp(-i\omega t)$ being the only time dependence is undermined (due to, for instance, two-stream instabilities). We assume here that no particle is slowed down to zero velocity in the laboratory frame, hence

$$\gamma(\vec{\eta}(t_0,t))m_0\left|\frac{\partial\xi(t_0,t)}{\partial t}\right|=\eta_z(t_0,t). \quad (12)$$

Substituting Eq. (12) into (10), the general form for the driving current becomes

$$\vec{J}(z,t)=-|e|n_0\nu_{z0}\int_{-\infty}^{\infty} \frac{\vec{\eta}(t_0,t)}{\eta_z(t_0,t)}\,\delta(t - \tau(t_0,z))dt_0. \quad (13)$$

Substituting the above form for $\vec{J}(z,t)$ into the right-hand side of Eqs. (7), we obtain the self-consistent amplitudes and phases of the scattered potentials in terms of driving currents. To show how the right-hand sides of Eqs. (7) can be reduced by using Eq. (13), we simplify Eq. (7a) as an illustration.

Substituting the x component of Eq. (13) into (7a) gives

$$\left(\frac{\omega^2}{c^2} - k_+^2(z)\right)A_x(z)$$

$$=\int_0^{2\pi/\omega} dt\int_{-\infty}^{\infty} dt_0\, G_x(t_0,z,t)\delta(t - \tau(t_0,z)), \quad (14a)$$

where

$$G_x(t_0,z,t)=4\frac{\omega}{c}\,|e|n_0\nu_{z0}\frac{\eta_x(t_0,t)}{\eta_z(t_0,t)}\cos\psi(z,t). \quad (14b)$$

Since the system of particles and fields is in the temporal steady state, particles which cross the $z = 0$ plane separated in time by $2\pi/\omega$ will execute identical orbits which are separated in time by

$2\pi/\omega$. It is therefore possible to define an initial beam segment, "beamlet," for which all possible steady-state orbits of the actual beam particles are represented by the particles in the beamlet, but are displaced in time. The axial length of the beamlet is clearly $2\pi v_{z0}/\omega$. With these considerations in mind we find that the functions $G_x(t_0,z,t)$ and $\tau(t_0,z)$ have certain periodic properties in their arguments which permit the integrals in Eq. (14) to be greatly simplified. Specifically we note that

$$G_x(t_0,z,t) = G_x(t_0 + 2\pi N/\omega, z, t + 2\pi N/\omega), \quad (15a)$$

and

$$\tau(t_0,z) = \tau(t_0 + 2\pi N/\omega, z) - 2\pi N/\omega, \quad (15b)$$

where $N = 0, \pm 1, \pm 2, \ldots$. The t integration in Eq. (14a) is over one wave period from 0 to $2\pi/\omega$. From Eq. (15b) we see that over this range of t the argument of the δ function will vanish over an interval in t_0 equal to $2\pi/\omega$. Therefore it is not necessary to integrate over t_0 from $-\infty$ to $+\infty$. Finally, from the property of $G_x(t_0,z,t)$ expressed in (15a) we find that

$$\int_0^{2\pi/\omega} dt \int_{-\infty}^{\infty} dt_0\, G_x(t_0,z,t)\delta(t - \tau(t_0,z))$$

$$= \int_0^{2\pi/\omega} G_x(t_0,z,\tau(t_0,z))\,dt_0. \quad (16)$$

This can be seen most easily in a diagram of the region of integration in Fig. 2, where the entire (t,t_0) plane is broken into squares of $2\pi/\omega$ on a side. Because of the symmetry property expressed in Eqs. (15a) and (15b), the value of the integrand is unchanged along a diagonal; this is indicated by certain squares having the same letter. Clearly then, an integral in the vertical direction, over the shaded squares, is the same as an integral in the horizontal direction, over the slashed squares. Substituting Eq. (16) together with (14b) into (14a) results in a simplified form for Eq. (7a). All the

integrals on the right-hand side of Eqs. (7) can be reduced in exactly the same way. Doing this we find that Eqs. (7) can be put into the form

$$[\omega^2/c^2 - k_+^2(z)]A_x(z)$$

$$= 4|e|n_0 \frac{v_{z0}}{c}\omega \int_0^{2\pi/\omega} \frac{\eta_x(t_0,\tau(t_0,z))}{\eta_z(t_0,\tau(t_0,z))}$$

$$\times \cos\psi(z,\tau(t_0,z))\,dt_0, \quad (17a)$$

$$2k_+^{1/2}(z)\frac{\partial}{\partial z}[A_x(z)k_+^{1/2}(z)]$$

$$= -4|e|n_0 \frac{v_{z0}}{c}\omega \int_0^{2\pi/\omega} \frac{\eta_x(t_0,\tau(t_0,z))}{\eta_z(t_0,\tau(t_0,z))}$$

$$\times \sin\psi(z,\tau(t_0,z))\,dt_0, \quad (17b)$$

$$[\omega^2/c^2 - k_+^2(z)]A_y(z)$$

$$= -4|e|n_0 \frac{v_{z0}}{c}\omega \int_0^{2\pi/\omega} \frac{\eta_y(t_0,\tau(t_0,z))}{\eta_z(t_0,\tau(t_0,z))}$$

$$\times \sin\psi(z,\tau(t_0,z))\,dt_0, \quad (17c)$$

$$2k_+^{1/2}(z)\frac{\partial}{\partial z}[A_y(z)k_+^{1/2}(z)]$$

$$= -4|e|n_0 \frac{v_{z0}}{c}\omega \int_0^{2\pi/\omega} \frac{\eta_y(t_0,\tau(t_0,z))}{\eta_z(t_0,\tau(t_0,z))}$$

$$\times \cos\psi(z,\tau(t_0,z))\,dt_0, \quad (17d)$$

$$\frac{\partial \phi(z)}{\partial z} = -4|e|n_0 v_{z0} \int_0^{2\pi/\omega} \sin\psi_z(z,\tau(t_0,z))\,dt_0, \quad (17e)$$

$$k(z)\phi(z) = -4|e|n_0 v_{z0}\int_0^{2\pi/\omega} \cos\psi_z(z,\tau(t_0,z))\,dt_0. \quad (17f)$$

Notice that on the right-hand side of the above equations the single integrals over t_0 are from 0 to $2\pi/\omega$. As we will see, these integrals can be evaluated numerically by following the orbits of a relatively small number of particles which enter the interaction region in any single time interval of duration $2\pi/\omega$. Upon deriving the general orbit equations for the particle ensemble in Sec. IV, we will assume that the scattered electromagnetic wave is circularly polarized, i.e., $A_x(z) = A_y(z)$. This assumption is clearly not central to our formulation.

FIG. 2. Diagram to illustrate the symmetry property of the function $\vec{G}(t_0,z,t)$ in the (t,t_0) plane.

IV. PARTICLE ORBIT EQUATIONS

We now express the particle orbits, which are needed for the evaluation of Eqs. (17), in terms of the new independent variables t_0 and z. The forces exerted on the electrons arise from the pump and scattered potentials given in Eqs. (1) and (4). We immediately note that the transverse canonical momenta of the particles are conserved. Therefore, if both the pump and scattered fields are zero as $z \to -\infty$, the transverse particle momenta are given by

$$p_x(z,t) = (|e|/c)[A_{0x}(z) + A_x(z,t)] \tag{18a}$$

and

$$p_y(z,t) = (|e|/c)[A_{0y}(z) + A_y(z,t)]. \tag{18b}$$

Using Eqs. (18), the longitudinal component of the force quation can be put into the form

$$\frac{dp_z(z,t)}{dt} = \frac{-|e|^2}{2\gamma(z,t)m_0 c^2}\left(\frac{\partial}{\partial z}[\vec{A}_0(z) + \vec{A}(z,t)]^2\right.$$
$$\left. -2\gamma(z,t)\frac{m_0 c^2}{|e|}\frac{\partial}{\partial z}\phi(z,t)\right), \tag{19}$$

where $p_z(z,t)$ is the axial momentum, and the relativistic γ factor is

$$\gamma(z,t) = \left(1 + \frac{|e|^2}{m_0^2 c^4}[\vec{A}_0(z) + \vec{A}(z,t)]^2 + \frac{p_z^2(z,t)}{m_0^2 c^2}\right)^{1/2}. \tag{20}$$

Equations (18)–(20) specify the particle dynamics in terms of the pump and scattered fields. The transverse and longitudinal particle motion is formally decoupled. To write Eqs. (18) and (19) in terms of the new independent variables z and t_0, we note that

$$t = \tau(t_0, z) = t_0 + \int_0^z dz'/v_z(t_0, z'),$$

$$\frac{d}{dt} = V_z(z,\tau)\frac{d}{dz},$$

where $V_z(z,\tau) = v_z(t_0, z)$. Note that d/dz (which follows a particle orbit) $\neq \partial/\partial z$ (which is taken at constant time).

In terms of z and τ we simply get

$$p_x(z,\tau) = (|e|/c)[A_{0x}(z) + A_x(z,\tau)], \tag{21a}$$

$$p_y(z,\tau) = (|e|/c)[A_{0y}(z) + A_y(z,\tau)], \tag{21b}$$

$$\frac{dp_z^2(z,\tau)}{dz} = -\frac{|e|^2}{c^2}\left(\frac{\partial}{\partial z}[\vec{A}_0(z) + \vec{A}(z,\tau)]^2\right.$$
$$\left. -2\gamma(z,\tau)\frac{m_0 c^2}{|e|}\frac{\partial}{\partial z}\phi(z,\tau)\right). \tag{21c}$$

We have expressed the particle orbits in terms of the entry time t_0 and axial position z. Note that our definition of the momenta implies that $\eta_x(t_0, \tau) = p_x(z,\tau)$, $\eta_y(t_0, \tau) = p_y(z,\tau)$, and

$$\eta_z(t_0, \tau) = p_z(z,\tau) = \gamma(z,\tau)m_0 V_z(z,\tau).$$

At this point we take the scattered electromagnetic wave to be circularly polarized and set $A_x(z) = A_y(z) = A(z)$. To obtain the final set of equations for the amplitude $A(z)$ and wave number $k_+(z)$ we first combine Eqs. (17a) and (17b) with Eqs. (17c) and (17d), respectively. Using the expressions for η_x and η_y given by Eqs. (21a) and (21b), we arrive at the expressions

$$[\omega^2/c^2 - k_+^2(z)]A(z)$$
$$= \frac{\omega_b^2}{2c^2}m_0 v_{z0}\frac{\omega}{\pi}\int_0^{2\pi/\omega}\eta_z^{-1}(t_0, \tau(t_0,z))\left[A_0(z)\cos\left(\int_0^z[k_+(z') + k_0(z')]dz' - \omega\tau(t_0,z) + \theta\right) + A(z)\right]dt_0, \tag{22a}$$

$$2k_+^{1/2}(z)\frac{\partial}{\partial z}[A(z)k_+^{1/2}(z)]$$
$$= -\frac{\omega_b^2}{2c^2}m_0 v_{z0}\frac{\omega}{\pi}\int_0^{2\pi/\omega}\eta_z^{-1}(t_0, \tau(t_0,z))\left[A_0(z)\sin\left(\int_0^z[k_+(z') + k_0(z')]dz' - \omega\tau(t_0,z) + \theta\right)\right]dt_0, \tag{22b}$$

where we have used Eqs. (1) and (4a) for $\vec{A}_0(z)$ and $\vec{A}(z,t)$ and $\omega_b = (4\pi|e|^2 n_0/m_0)^{1/2}$.

For completeness we rewrite Eqs. (17e) and (17f) for the scalar potential

$$\frac{\partial\phi(z)}{\partial z} = \frac{-\omega_b^2}{c^2}\frac{v_{z0}}{\pi}\frac{m_0 c^2}{|e|}$$
$$\times\int_0^{2\pi/\omega}\sin\left(\int_0^z k(z')dz' - \omega\tau(t_0,z) + \theta_z\right)dt_0, \tag{23a}$$

$$k(z)\phi(z) = \frac{-\omega_b^2}{c^2}\frac{v_{z0}}{\pi}\frac{m_0 c^2}{|e|}$$
$$\times\int_0^{2\pi/\omega}\cos\left(\int_0^z k(z')dz' - \omega\tau(t_0,z) + \theta_z\right)dt_0. \tag{23b}$$

The relevant particle dynamics is contained in Eq.

(21b), which is rewritten in the form

$$\frac{d\eta_z^2(t_0,\tau)}{dz} = \frac{-|e|^2}{c^2}\left(\frac{\partial}{\partial z}[\vec{A}_0(z)+\vec{A}(z,\tau)]^2\right.$$

$$\left. -2\gamma(z,\tau)\frac{m_0c^2}{|e|}\frac{\partial\phi(z,\tau)}{\partial z}\right), \quad (24)$$

where

$$\gamma(z,\tau) = \left(1 + \frac{|e|^2}{m_0^2c^4}[\vec{A}_0(z)+\vec{A}(z,\tau)]^2 + \frac{\eta_z^2(t_0,\tau)}{m_0^2c^2}\right)^{1/2}, \quad (25a)$$

$$\tau(t_0,z) = t_0 + \int_0^z \frac{\gamma(z',\tau(t_0,z'))m_0}{\eta_z(t_0,\tau(t_0,z'))}dz', \quad (25b)$$

$$[\vec{A}_0(z)+\vec{A}(z,\tau)]^2 = A_0^2(z)+A^2(z)+2A_0(z)A(z)$$

$$\times\cos\left(\int_0^z[k_+(z')+k_0(z')]dz'\right.$$

$$\left. -\omega\tau+\theta\right). \quad (25c)$$

The nonlinear formulation of the FEL is fully described by Eqs. (22)–(24). The ponderomotive potential plays a central role in axially bunching the electron. From Eq. (24) we see that this potential is given by

$$\phi_{\text{pond}}(z,\tau) = \frac{-|e|}{\gamma_0}\frac{A_0(z)A(z)}{m_0c^2}$$

$$\times\cos\left(\int_0^z[k_+(z')+k_0(z')]dz'\right.$$

$$\left. -\omega\tau+\theta\right). \quad (26)$$

The amplitude and phase of the scattered fields as well as the axial beam momentum all vary with a characteristic axial length which is much longer than the pump wavelength l. This fact allows inexpensive numerical simulations to be performed in the laboratory frame with extremely high-γ electron beams.

To see that the system quantities vary on a scale length long compared to l, we note that the characteristic length, as estimated from the arguments of the sinusoidal terms on the right-hand side of Eqs. (22)–(24), is roughly equal to L $\approx(k_+ + k_0 - \omega/\nu_z)^{-1}$. However, since the frequency of the scattered radiation is $\omega = (1+\beta_z)\gamma_z^2\nu_z k_0$, we find that

$$L \gg 1/k_0 = l/2\pi.$$

This fact permits us to solve numerically the FEL equations for arbitrarily high-γ beams. The more conventional simulation approaches suffer from the problem of large temporal or spatial scale differences even in the beam frame of reference.

To complete our formulation of FEL we need an expression for the efficiency. The efficiency can be defined as the ratio of the electromagnetic-energy-flux increase to the initial electron-energy flux, that is,

$$\eta = \frac{c}{4\pi}\frac{\langle\vec{E}(z,t)\times\vec{B}(z,t)\rangle_t - \langle\vec{E}(0,t)\times\vec{B}(0,t)\rangle_t}{\nu_{z0}n_0(\gamma_0-1)m_0c^2}, \quad (27)$$

where $\vec{E} = c^{-1}\partial\vec{A}/\partial t$, $\vec{B} = \hat{e}_z\times\partial\vec{A}/\partial z$, $\langle\cdots\rangle_t$ denotes an average over the field period $2\pi/\omega$, and ν_{z0}, n_0, and γ_0 are the initial beam axial velocity, density, and total γ factor.

Using the vector potential in Eq. (4a) and taking the radiation field to be circularly polarized, i.e., $A_x = A_y = A$, the efficiency in Eq. (27) takes the form

$$\eta = \left(\frac{|e|}{m_0c}\right)^2\frac{\omega}{\omega_b^2}\frac{[k_+(z)A^2(z)-k_+(0)A^2(0)]}{\nu_{z0}(\gamma_0-1)} \quad (28)$$

and is maximum when the radiation fields saturate.

V. DERIVATION OF LINEAR GROWTH RATES, EFFICIENCIES, AND SATURATION-FIELD AMPLITUDES

In this section we present the salient features of the FEL in the linear regime. Results for the linear growth rate and expressions for the saturation efficiency and radiation amplitude are obtained in the high-gain case, i.e., where the radiation-field amplitude has e folded at least a few times. For a more detailed derivation of these quantities see Refs. 17 and 18.

In the high-gain linear regime the excited space charge and vector potentials are of the form

$$\phi(z,t) = \tfrac{1}{2}\tilde{\phi}(0)e^{i(kz-\omega t)} + \text{c.c.},$$

$$\vec{A}(z,t) = \tfrac{1}{2}\tilde{A}(0)e^{i(k_+z-\omega t)}(\hat{e}_x+i\hat{e}_y) + \text{c.c.}, \quad (29)$$

where $\tilde{\phi}(0)$ and $\tilde{A}(0)$ are the potential amplitudes at the input end of the interaction region, $z=0$ and the wave numbers k and k_+ are complex and independent of z. For a magnetic pump of the form in Eq. (1) with constant amplitude and period and cold-electron beam, the dispersion relation is

$$D(\omega,k_+)[(\omega-\nu_{z0}k)^2 - \omega_b^2/\gamma_{z0}^2\gamma]$$

$$= -(\omega_b^2/2\gamma_0)(\beta_{z0}\beta_{0\perp})^2D(\omega,k), \quad (30)$$

where $D(\omega,k) = \omega^2 - c^2k^2 - \omega_b^2/\gamma_0$, $k_+ = k - k_0$, k_0 is the pump wave number, $\omega_b = (4\pi|e|^2n_0/m_0)^{1/2}$ is the beam plasma frequency, ν_{z0} is the axial beam velocity, $\nu_{0\perp} = |e|B_0/(\gamma_0m_0ck_0)$ is the transverse beam velocity, B_0 is the pump amplitude, γ_0 $= (1-\beta_{z0}^2-\beta_{0\perp}^2)^{-1/2}$, $\beta_{0\perp} = \nu_{0\perp}/c$, $\beta_{z0} = \nu_{z0}/c$, and γ_{z0} $= (1-\beta_{z0}^2)^{-1/2}$. Since the electromagnetic wave approximately satisfies the dispersion relation ω/c $\approx k_+$ we can replace $D(\omega,k_+)$ and $D(\omega,k)$ by

$-2k_+[k_+ - (\omega^2 - \omega_b^2/\gamma_0)^{1/2}/c]$ and $-2kk_0c^2$, respectively. The dispersion relation can now be put into the simple form

$$\delta k(\delta k + 2\xi k_0/\gamma_{z0})(\delta k - \Delta k) = -\tfrac{1}{2}\alpha^2 k_0, \qquad (31)$$

where $k = \omega/\nu_{z0} + \xi k_0/\gamma_{z0} + \delta k$, δk is complex, $|\delta k| \ll k$, $\xi = \omega_b/(\sqrt{\gamma_0}\,ck_0)$, $\Delta k = k_0 - \omega/(2c\gamma_{z0}^2)$, and $\alpha^2 = (\xi\beta_{0\perp}k_0)^2$. Equation (31) assumes that the beam is relativistic, $\nu_{z0} \approx c$, and $\omega \gg \omega_b/\sqrt{\gamma_0}$. Two distinct regimes can be distinguished from the dispersion relation in Eq. (31).

A. Weak-magnetic-pump limit

For a pump magnetic field strength such that $\beta_{0\perp} \ll \beta_{crit} \equiv 4(\xi/\gamma_{z0}^3)^{1/2}$ the space-charge potential dominates the ponderomotive potential and collective effects play an important role. In this regime of scattering the dispersion relation in Eq. (31) yields

$$\delta k = \tfrac{1}{2}\Delta k - \tfrac{1}{2}i[\alpha^2\gamma_{z0}/\xi - (\Delta k)^2]^{1/2} \qquad (32)$$

for the growing root. Maximum spatial linear growth occurs when there is no frequency mismatch, i.e., $\Delta k = 0$, and is given by

$$\Gamma_{max} = -\text{Im}(\delta k)_{max} = \tfrac{1}{2}(\alpha^2\gamma_{z0}/\xi)^{1/2}. \qquad (33)$$

B. Strong-magnetic-pump limit

In this regime, defined by the condition $\beta_{0\perp} \gg \beta_{crit}$, space-charge forces are dominated by ponderomotive forces. This is a single-particle scattering regime and Eq. (31) reduces to

$$(\delta k)^2(\delta k - \Delta k) = -\tfrac{1}{2}\alpha^2 k_0. \qquad (34)$$

The maximum spatial linear growth rate according to Eq. (34) occurs for exact frequency matching, i.e., $\Delta k = 0$, and is given by

$$\Gamma_{max} = -\text{Im}(\delta k)_{max} = (\sqrt{3}/2^{4/3})(\xi\beta_{0\perp})^{2/3}k_0. \qquad (35)$$

To obtain estimates for the saturation levels in the high-gain regimes we resort to heuristic arguments based on electron-trapping dynamics. It can be argued that at saturation, when electrons are deeply trapped, the axial velocity of the electron beam has decreased by the amount $2\Delta\nu$ where $\Delta\nu = \nu_{z0} - \nu_{ph}$ is the difference between the equilibrium axial beam velocity and the initial phase velocity of the total longitudinal wave, i.e., $\nu_{ph} = \omega/\text{Re}(k)$. The decrease in the particle kinetic energy is

$$\Delta E_{KE} \approx 2\gamma_0\gamma_{z0}^2 m_0\nu_{z0}\Delta\nu, \qquad (36)$$

so the energy conversion efficiency becomes

$$\eta = [\Delta E_{KE}/(\gamma_0 - 1)m_0c^2] \approx 2\gamma_{z0}^2\Delta\nu/c$$
$$= 2\gamma_{z0}^2[\nu_{z0} - \omega/\text{Re}(k)]/c. \qquad (37)$$

Substituting

$$\text{Re}(k) = \omega/\nu_{z0} + \xi k_0/\gamma_{z0} + \text{Re}(\delta k)$$

and $\omega \approx 2\gamma_{z0}^2 ck_0$ into Eq. (37), the expression for efficiency becomes

$$\eta = \xi/\gamma_{z0} + \text{Re}(\delta k)/k_0, \qquad (38)$$

where $\text{Re}(\delta k)$ is determined from the solution of the dispersion relation in Eq. (31). Using Eqs. (31) and (38) we find that in the weak-pump and strong-pump limit the growth rate maximizes when $\Delta k = 0$, i.e., $\omega = 2\gamma_{z0}^2 ck_0$, and the efficiencies at saturation are, respectively,

$$\eta = \xi/\gamma_{z0} \qquad (39)$$

and

$$\eta = 2^{-4/3}(\xi\beta_{0\perp})^{2/3} + \xi\gamma_{z0}. \qquad (40)$$

Applying the conservation law for total energy flux we find that the magnitude of the vector potential at saturation is

$$|\vec{A}_{sat}| = (\xi\gamma_0/2\gamma_{z0}^2)(m_0c^2/|e|)\eta^{1/2}, \qquad (41)$$

where η is given by either Eq. (39) or (40), depending on whether the weak- or strong-pump limit is applicable.

VI. RESULTS AND DISCUSSION

In this section we present the numerical results for the coupled nonlinear FEL equations in Eqs. (22)–(24). Illustrations for a wide range of parameters ranging from the submillimeter to the optical radiation regime are given. The mono-energetic electron beam enters the interaction region at $z = 0$ with a uniform density. The magnetic-pump field given in Eq. (1) is assumed to be built up adiabatically from $z \le 0$ to its initial value at $z = 0$. In all of our numerical simulations a small-amplitude radiation field is introduced as a perturbation at $z = 0$ and allowed to grow spatially and self-consistently according to the FEL equations. The small initial radiation field, typically less than 0.1% of the saturated-field amplitude, allows for a long spatial region of linear interaction and hence for an accurate comparison with the linear theory presented in Sec. V. Furthermore, space-charge fields are included in all of our numerical illustrations even though in some cases the ponderomotive field may dominate the process, as is the case in the strong-magnetic-pump scattering limit.

We will first consider two examples where the magnetic-pump parameters are fixed, i.e., constant amplitude and period. Furthermore, we will show that efficiency can be increased to a few 10's of percent even in the optical regime by

TABLE I. Optical and submillimeter illustrations of FEL's (constant-magnetic-pump parameters).

		Example #1	Example #2
Magnetic-pump parameters			
Pump wavelength	l	1.5 cm	2.0 cm
Pump amplitude	B_0	6.0 kG	2.5 kG
Electron-beam parameters			
Beam energy	E_0	66 MeV $(\gamma_0 = 131)$	2.6 MeV $(\gamma_0 = 6)$
Beam current	I_0	2 kA	5 kA
Axial gamma	γ_{z0}	100	5.4
Beam radius	r_0	0.1 cm	0.3 cm
Equil. $\perp$ velocity	$\beta_{0\perp}$	6.4×10^{-3}	0.078
Critical $\perp$ velocity	β_{crit}	1.5×10^{-3}	0.22
Beam strength parameter	ξ	0.14	0.87
Self-potential-energy spread	$\Delta E/E_0$	0.08%	1.7%
Output-radiation parameters			
Radiation wavelength	λ	0.75 μ	338 μ
Linear e-folding length [a]	$L_e = -\text{Im}(k)^{-1}$	38 cm	5.3 cm
Efficiency [a]	η	0.52%	9.2%
Saturated A field [a]	A	33 V	7.4×10^3 V
Radiation power [a]	P_0	0.69 GW	1.2 GW

[a] For maximum growth rate.

contouring the magnetic-pump period and amplitude.

A. Constant-magnetic-pump illustrations

Two examples will be discussed in some detail: (i) optical radiation at $\lambda = 0.75$ μ from a 66-MeV electron beam and (ii) submillimeter radiation at $\lambda = 338$ μ with a 2.6-MeV electron beam. Table I lists the salient parameters for the magnetic pump, electron beam and output radiation of both examples.

For the optical radiation case, example 1, the magnetic-pump amplitude is 6.0 kG and the period is fixed at 1.5 cm. The 66-MeV $(\gamma_0 = 131)$, 2-kA electron beam has a transverse equilibrium velocity of $v_{0\perp} = 6.4 \times 10^{-3}$ c with the given value of magnetic-pump field. The critical transverse velocity, see Sec. V, is $v_{crit} = 1.5 \times 10^{-3} c$, hence the scattering process is in the strong-pump regime.

Figure 3 shows the amplitude of the vector potential of the scattered radiation $A(z)$ and the spatial growth rate $\Gamma = \partial[\ln A(z)]/\partial z$ as a function of z. Those plots are for an optical frequency of $\omega = 2\gamma_{z0}^2 ck_0 = 2.525 \times 10^{15}$ sec^{-1}. Notice that in Fig. 3 there is a long spatial region where the growth rate is fairly constant. This is the linear region of the interaction. The value of the radiation frequency in this figure has been chosen to maximize the linear growth rate, i.e., zero frequency mismatch, $\Delta k = 0$. The linear e-folding length asso-

ciated with this output frequency is 38 cm.

Figure 4 shows a comparison between the spatial growth rates obtained from the linear regime of the numerical simulation of our FEL equations [crosses $(\times)$] and the linear growth rates obtained from the dispersion relation in Eq. (30), (solid curve) over the frequency spectrum. These two independent calculations of the linear growth rate are in excellent agreement. Figure 4 also compares the efficiency at saturation obtained by solving the FEL equations [circles $(\bigcirc)$] with the calculated values of efficiency using electron-trapping arguments (dotted curve) given in Sec. V.
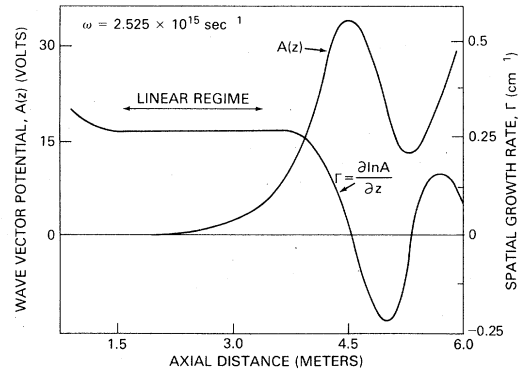
FIG. 3. Wave vector potential $A(z)$ and spatial linear growth rate Γ as a function of axial distance for example 1 in the optical regime. The frequency is chosen to give the maximum linear spatial growth rate.
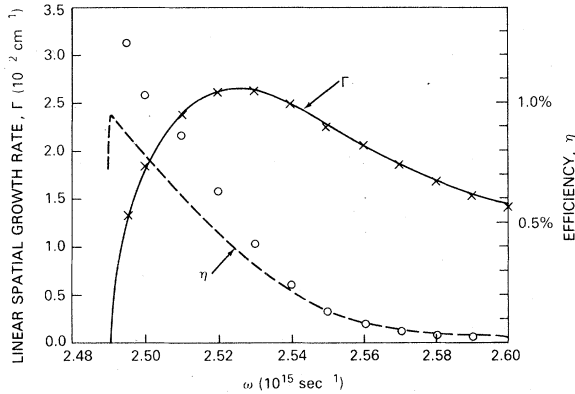
FIG. 4. A comparison of the growth rate in the linear regime of the nonlinear simulation [crosses (✕)] with the growth rate from linear theory (solid curve), and a comparison of efficiency from nonlinear theory [circles (○)] with that from linear theory using trapping arguments (dashed curve) as a function of frequency for example 1.

Using the value of efficiency for maximum linear growth rate, we find from Eq. (41) that the saturated vector-potential amplitude is $A_{sat} = 28$ V, corresponding to an efficiency of 0.37%, whereas Fig. 3 gives a value of 33 V for A_{sat}, corresponding to an efficiency of 0.52%. The higher calculated efficiency can be explained by the slight increase of the wave number k_+ of the scattered radiation just before saturation, as shown by the solid curve in Fig. 5. When k_+ increases, the phase velocity of the ponderomotive potential $\omega/[k_+(z) + k_0(z)]$ decreases. As the electrons become trapped at the bottom of the potential well, the ponderomotive wave slows down slightly; hence, the particles are able to transfer more kinetic energy to the scattered radiation. This
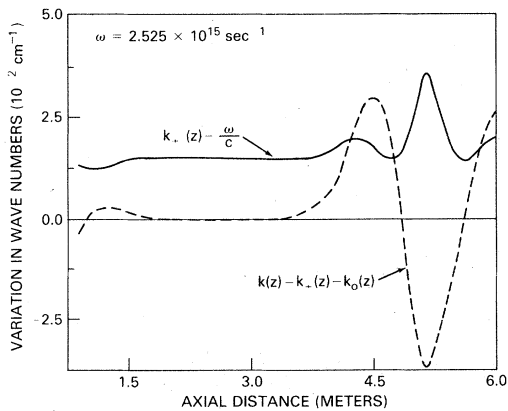
FIG. 5. The variation of wave number of the scattered radiation $k_+(z)$ and the variation in wave number of the space-charge potential $k(z)$ as a function of axial distance for example 1 at the frequency corresponding to maximum linear spatial growth.
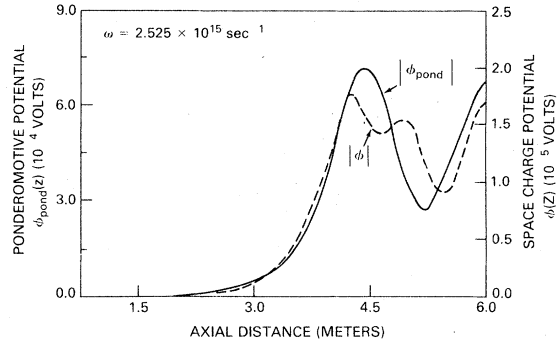
FIG. 6. A comparison of the magnitude of the ponderomotive potential $|\phi_{pond}(z)|$ and the space-charge potential $|\phi(z)|$ as a function of axial distance for example 1 at the frequency corresponding to maximum linear spatial growth.

is clearly a nonlinear effect, which linear theory could not predict. The dotted curve in Fig. 5 is the variation of the wave number of the space-charge wave. The effects of the space-charge wave is negligible, since in the strong-pump limit, example 1, the ponderomotive potential is much larger than the space charge potential, as can be seen in Fig. 6.

To understand the phenomenon of trapping, phase-space plots are a revealing tool. Figures 7(a)–7(d) are plots of the relative time the particles in one beamlet cross the following axial positions: $z = 0.0$, 2.0, 4.0, 4.3, and 4.5 m. Twenty particles are labeled within the beamlet. At the initial position, $z = 0$, the particles enter at equal intervals in time since they have uniform axial velocity v_{z0}. At $z = 2$ m, downstream into the interaction region, the particles are in the linear regime where the growth rate of the scattered radiation is constant. Some particles have gained energy while others have lost energy depending on their phase relation with the ponderomotive potential. At $z = 4$ m, Fig. 7(b), the phase-space plot begins to show the signs of trapping. Many of the particles are crossing the $z = 4$ m plane at about the same time. However, their velocity spread is large. Figure 7(c), at $z = 4.3$ m, depicts the particles before saturation and shows definite signs of trapping. At $z = 4.5$ m, particles labeled 4–9 in Fig. 7(d) show spatial bunching and small velocity spread; these particles are deeply trapped. If the amplitude and period of the magnetic-pump field is held fixed, the scattered radiation will reach its maximum value at this axial position.

Our nonlinear formulation is also applied to a case where the output radiation is in the submillimeter regime, example 2 in Table I. The pump wavelength and pump magnetic field amplitude are
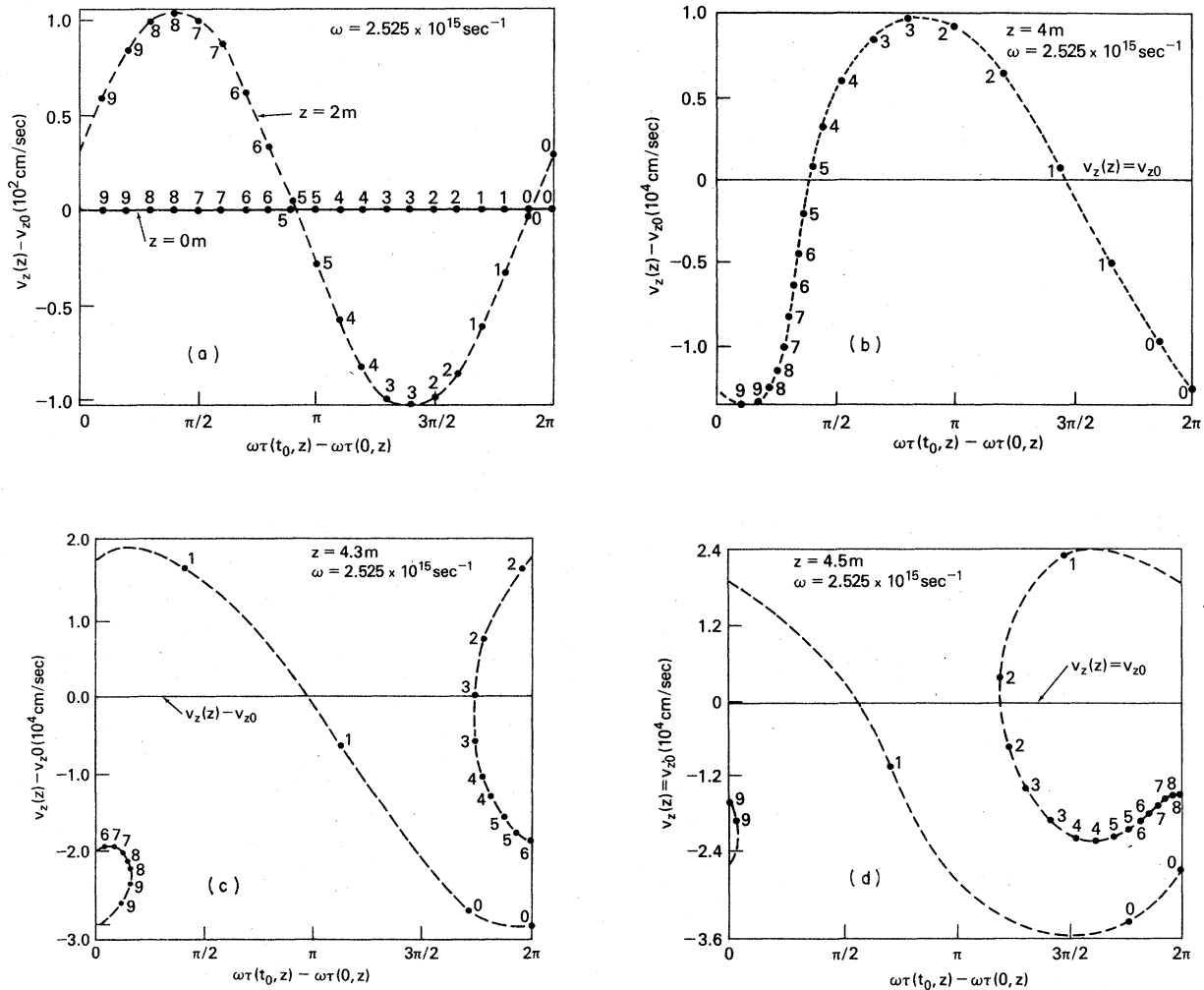
FIG. 7. Phase-space plots of velocity vs the relative time the particles in one beamlet cross the following axial positions: (a) $z = 0.0$ and 2.0 m . (b) $z = 4.0$ m, (c) $z = 4.3$ m, and (d) $z = 4.5$ m for example 1.
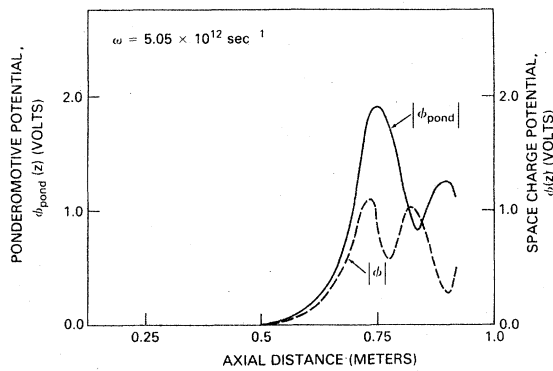
FIG. 8. Comparison of the magnitude of the pondero-motive potential $| \phi_{pond}$ $(z) |$ and the space-charge potential $| \phi(z) |$ as a function of axial distance for example 2 at the frequency corresponding to maximum linear spatial growth.
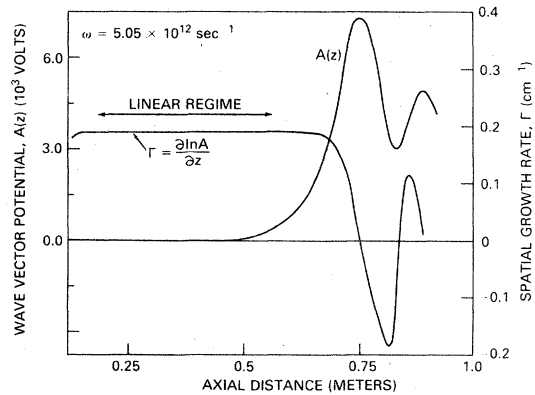
FIG. 9. Wave vector potential $A(z)$ and spatial growth rate Γ as a function of axial distance for example 2 at the frequency corresponding to maximum linear growth.

2 cm and 2.5 kG, respectively. The electron-beam energy is 2.6 MeV ($\gamma_0 = 6$); the beam current is 5 kA and the beam radius is 0.3 cm. The transverse equilibrium velocity is $v_{0\perp} = 0.078c$, and the critical transverse velocity is $v_{\text{crit}} = 0.22c$. In the example we are barely in the weak-pump regime, since β_{crit} is less than three times $\beta_{0\perp}$. Space-charge effects are, therefore, important in this example. Figure 8 is a plot of the space charge and ponderomotive potential for $\omega = 5.05 \times 10^{12}$ sec^{-1} ($\lambda = 338$ μ). This figure shows that collective effects are of the same order of magnitude as the ponderomotive forces.

Figure 9 shows the amplitude of the vector-potential amplitude of the scattered radiation, $A(z)$, and the spatial growth rate $\Gamma = \partial[\ln A(z)]/\partial z$ as a function of z for $\omega = 5.05 \times 10^{12}$ sec^{-1}.

Comparing the linear spatial growth rate obtained from the dispersion equation (30) (solid curve in Fig. 10) with the growth rate from the linear regime of the nonlinear calculation [cross ($\times$)], we again obtain excellent agreement. The theoretical efficiency based on Eqs. (38) and (31) (dotted curve in Fig. 10) as compared with the results using the nonlinear formulation [circles ($\bigcirc$)] is remarkably good. The changes in wave number of the scattered radiation, $k_+(z)$, near saturation (solid curve in Fig. 11) did not enhance the efficiency because the effect is balanced by the increase in the space-charge-potential wave.

The particle phase-space plots of Figs. 12(a)–12(c), are very similar in nature to those in Figs. 7(a)–7(d). Figure 12(a) contains phase plots at $z = 0.0$ and 0.35 m corresponding to the initial position and a point in the linear interaction regime. At the $z = 0.7$ m plane just before saturation, Fig. 12(b) shows the beginning of particle
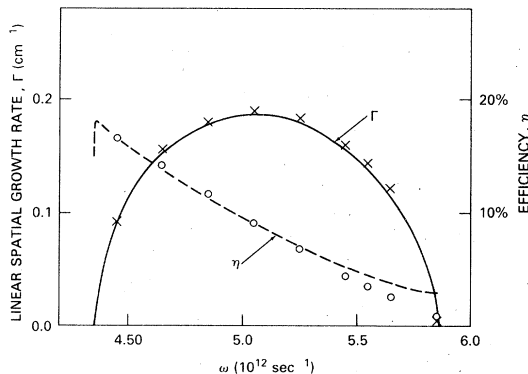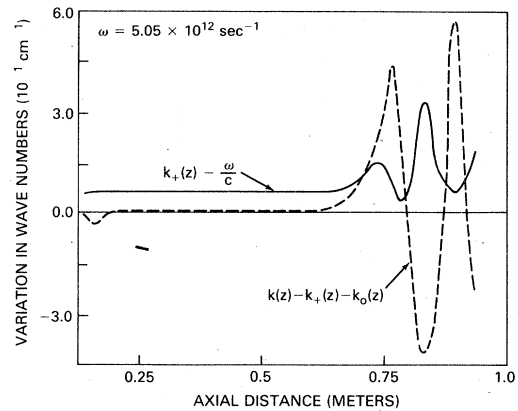
FIG. 11. Variation in wave number of the scattered radiation $k_+(z)$ and the variation in wave number of the space-charge potential $k(z)$ as a function of axial distance for example 2 at the frequency corresponding to maximum linear spatial growth.

trapping. Figure 12(c) contains the phase-space plot when the radiation field has saturated, $z = 0.77$ m.

Figure 13 shows the scaling of the linear spatial growth rate and maximum efficiency as a function of the pump magnetic field amplitude B_0 at a fixed output frequency. The output radiation frequency is held constant by requiring that γ_{z0} and k_0 be kept fixed. The electron-beam and magnetic-pump parameters are basically the same as those of example 1 in Table I, except that the magnetic-pump amplitude ranges from 0.25 to 6 kG. To keep the frequency fixed, while B_0 is varied, the electron-beam energy is changed such that γ_{z0} is held at the constant value of 100. The output frequency used for Fig. 13 is chosen at the maximum growth rate, which is very close to $\omega = 2\gamma_{z0}^2 ck_0 = 2.525 \times 10^{15}$ sec^{-1}, corresponding to a wavelength of $\lambda = 0.75$ μ. The critical transverse velocity, as discussed in Sec. V, occurs for these parameters at a pump magnetic field of $B_0 = 1.15$ kG. Above this value of pump field the FEL process is in the strong-pump regime, while sufficiently below $B_0 = 1.15$ kG the scattering process is in the weak-pump regime. In Fig. 13 the crosses ($\times$) denote the linear spatial growth rate obtained from the nonlinear simulations, while the solid curve is obtained from the dispersion relation in Eq. (30). Also in this figure is a comparison of efficiency estimated from Eq. (38) using trapping arguments (dashed curve) and actual numerical simulation results [circles ($\bigcirc$)].

B. Efficiency enhancement by contouring magnetic-pump period

According to Eqs. (24) and (26) the phase velocity of the total longitudinal-wave potential, i.e., pon-

FIG. 10. Comparison of the growth rate in the linear regime of the nonlinear simulation [crosses ($\times$)] with the growth rate from linear theory (solid curve), and a comparison of efficiency from the nonlinear theory [circles ($\bigcirc$)] with that from linear theory using trapping arguments (dashed curve) as a function of frequency for example 2.
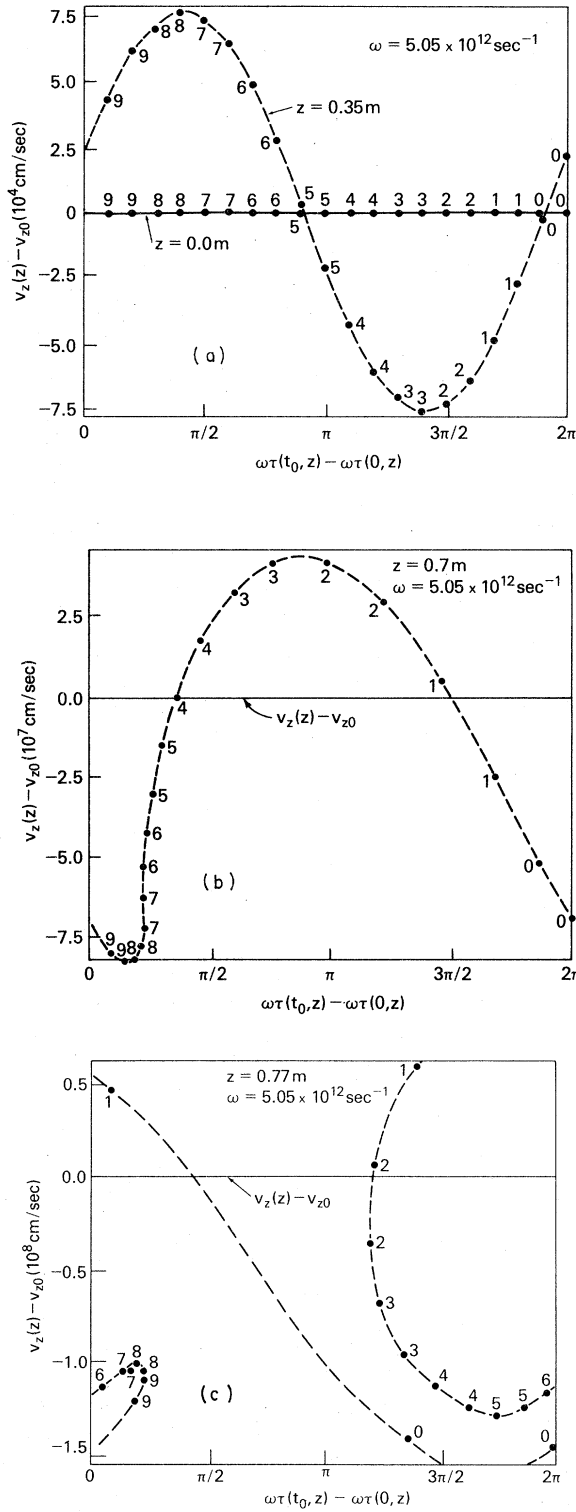
FIG. 12. Phase-space plots of velocity vs the relative time the particles in one beamlet cross the following axial positions: (a) $z = 0.0$ and 0.35 m, (b) $z = 0.7$ m, and (c) $z = 0.77$ m for example 2.
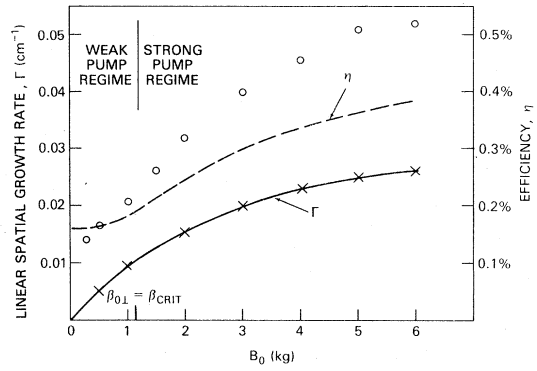
FIG. 13. Comparison of the maximum growth rate in the linear regime of the nonlinear simulation [crosses (✕)] with the maximum growth rate from linear theory (solid curve), and a comparison of efficiency from non-linear theory [circles (○)] with that from linear theory using the trapping arguments (dashed curve) as a function of the magnetic-pump field amplitude for a fixed output frequency.

deromotive plus space charge is

$$\nu_{ph} = \omega/(k_+ + k_0),\qquad(42)$$

where ω and k_+ are the radiation frequency and wave number and $k_0 = 2\pi/l$ is the wave number of the pump field. It has been assumed in writing Eq. (42) that the wave number of the ponderomotive and space-charge waves are identical. The longitudinal-wave potential is responsible for axially bunching and eventually trapping the electrons. If the magnetic-pump period is held fixed, the radiation field reaches its maximum value when the electrons are trapped at the bottom of the longitudinal potential wells, as can be seen for example in Fig. 7(d). Just before the radiation field saturates, the electrons are somewhat spatially bunched and trapped near the bottom of the wave potential [see Fig. 7(c)]. The trapped electrons at this point can be considered, for our purpose, to form a macroparticle. By appropriately reducing the phase velocity in Eq. (42) as a function of axial distance down the interaction region, the kinetic energy of this macroparticle can be further reduced and converted into wave energy. The phase velocity must be reduced in such a way so that the inertial potential of the trapped macroparticle is always less than the potential of the growing longitudinal wave. According to Eq. (42), the phase velocity can be reduced by decreasing the period of the magnetic pump as a function of z. In order for the macroparticle to remain trapped, the spatial rate of change of the pump period must be sufficiently slow. In principle virtually all the kinetic energy associated with axial motion of the macroparticle can be extracted and converted to
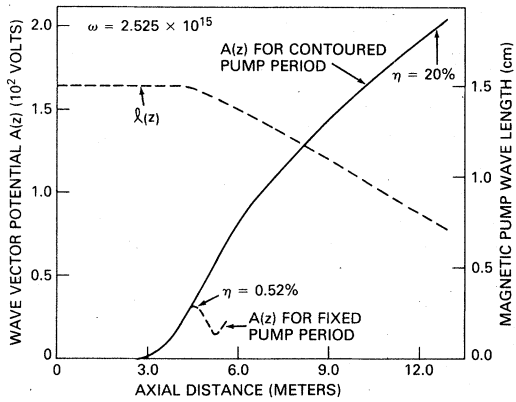
FIG. 14. Enhancement of radiation field by decreasing the magnetic-pump period and increasing the magnetic-pump amplitude. The efficiency has increased from 0.52% at $z = 4.5$ m with a constant pump period to 20% at $z = 13$ m with the period of the pump changing as shown.

wave energy. However, not all the beam particles comprise the macroparticle; some are untrapped. Converting particle kinetic energy into radiation by varying the wave velocity is somewhat analo-

gous to the reverse process of particle acceleration in, say, an rf linac. In a wave accelerator, the energy associated with the accelerating slow electromagnetic wave is converted into particle kinetic energy. However, the wave energy in these accelerators does not decay, since it is continuously resupplied by external microwave sources.

We will illustrate efficiency enhancement by contouring the pump period while holding the amplitude of the pump magnetic vector potential constant, using the parameters of example 1 in Table I. The same principle of efficiency enhancement can also be applied to example 2. Figure 7(c) shows that at $z = 4.3$ m, the electrons are somewhat spatially bunched at the optical wavelength $\lambda = 0.75$ μ and the radiation field is nearly saturated. At this point, we simply increased the pump wave number $k_0(z)$ exponentially as a function of z instead of optimally contouring the pump period. The period of the magnetic pump, $l(z)$, is depicted in Fig. 14. The spatial decrease of l results in a large increase in the amplitude of the wave vector potentials, as shown in Fig. 14.
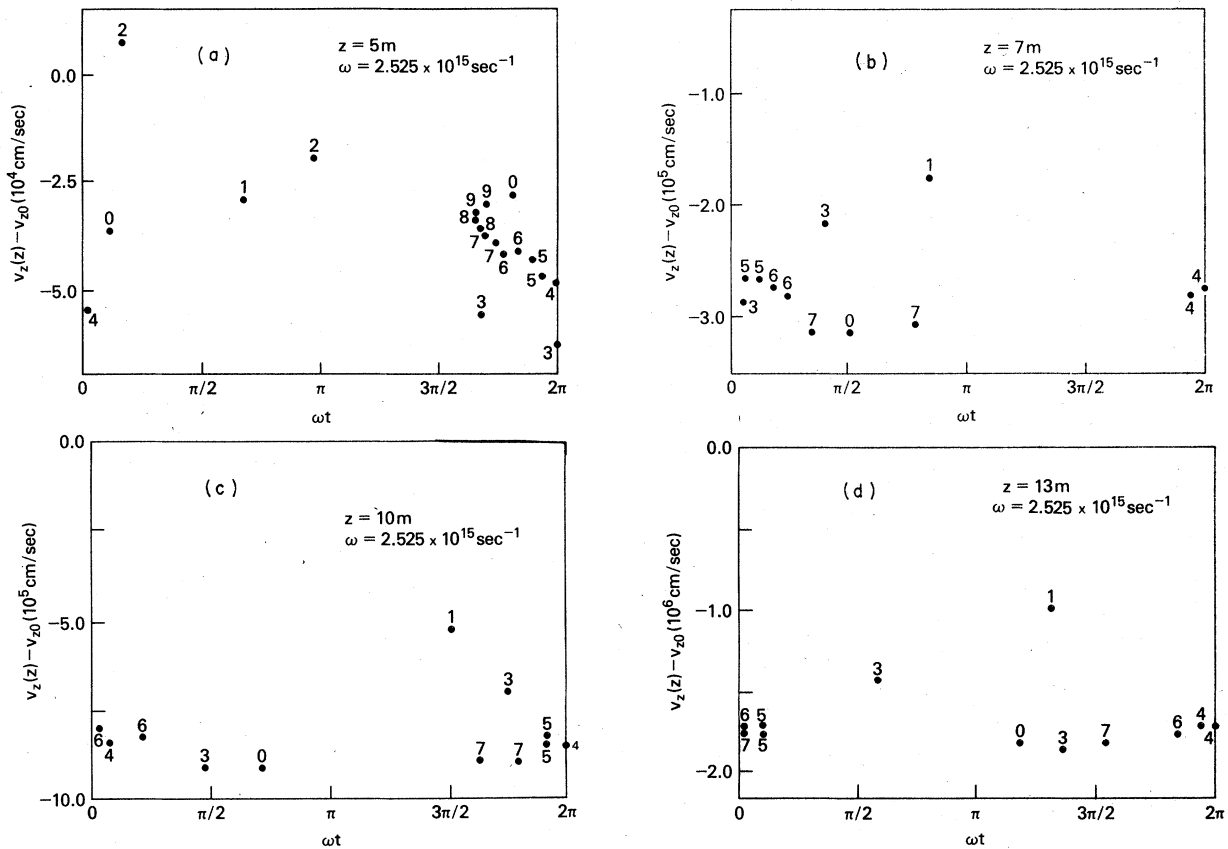
FIG. 15. Phase plots with contoured magnetic-pump period shown in Fig. (14) at (a) $z = 5$ m, (b) $z = 7$ m, (c) $z = 10$ m, and (d) $z = 13$ m.

For this particular case, the contouring is terminated at $z = 13$ m and the efficiency at this point is already 20%. In principle, the pump wavelength contouring can be continued and even higher efficiencies achieved. Figures 15(a)–15(d) are the phase plots with contouring at $z = 5$, 7, 10, and 13 m. At $z = 5$ m the majority of the particles are well bunched. At $z = 7$ m, 12 out of 20 particles are trapped by the ponderomotive potential wells; the same 12 particles remain trapped even at $z = 13$ m. Since the amplitude of the ponderomotive potential is proportional to the radiation field, it increases as the radiation field increases. Once the particles are trapped the particles remain trapped and continually lose energy if the pump period l is decreased adiabatically.

A number of alternative efficiency-enhancement schemes have been suggested.[36,37] One such approach is to fix the magnetic pump period while decreasing the magnetic pump amplitude.[36] The energy associated with motion in the perpendicular direction is converted to radiation energy. The maximum efficiency using this method is $\eta_{\max} = \alpha(\gamma_0 - \gamma_{z0})/(\gamma_0 - 1)$, where $\gamma_0 = \gamma_{\perp 0}\gamma_{z0}$ is the total initial relativistic γ factor, $\gamma_{\perp 0} = (1 + |e|^2 A_0^2/m_0^2 c^4)^{1/2}$, $\gamma_{z0} = [1 - (v_{z0}/c)^2]^{-1/2}$, and α is the fraction of trapped particles. The method of efficiency enhancement by increasing the wave number and the magnetic field of the pump converts the axial kinetic energy of the electrons to radiation energy. The maximum efficiency in principle is $\eta_{\max} = \alpha(\gamma_0 - \gamma_{\perp 0})/(\gamma_0 - 1)$. Since $\gamma_{z0} > \gamma_{\perp 0}$, it seems that the latter approach would lead to higher efficiencies.

APPENDIX: GENERAL NONLINEAR FORMULATION

In this appendix we outline the general formulation of the FEL equations, taking into account spa-

tial harmonics in the magnetic-pump field as well as spatial and temporal harmonics in the scattered fields. Furthermore, the polarization of the electromagnetic field is arbitrary and permitted to evolve according to the nonlinear particle field dynamics.

The vector potential of the periodic pump field containing spatial harmonics of variable amplitudes and wave numbers is expressed as

$$\vec{A}_0(z) = \sum_{m=1} A_{0,m}(z) \left[\cos\left(m \int_0^z k_0(z')dz'\right)\hat{e}_x + \sin\left(m \int_0^z k_0(z')dz'\right)\hat{e}_y \right],$$

(A1)

where the amplitude and fundamental wave number are slowly varying functions of z. This field is not curl free, but is a good approximation to the exact helically symmetric field near the $r = 0$ axis, when $mk_0 r_0 < 1$, where r_0 is the radius of the electron beam. The pump magnetic field associated with Eq. (A1) is given by

$$\vec{B}_0(z) = \sum_{m=1} B_{0,m}(z) \left[\cos\left(m \int_0^z k_0(z')dz' + \varphi_m(z)\right)\hat{e}_x + \sin\left(m \int_0^z k_0(z')dz' + \varphi_m(z)\right)\hat{e}_y \right],$$

where

$$B_{0,m}(z) = -\left[[mk_0(z)A_{0,m}(z)]^2 + \left(\frac{\partial A_{0,m}(z)}{\partial z}\right)^2 \right]^{1/2}$$

and

$$\varphi_m(z) = -\tan^{-1}\left[\left(\frac{\partial A_{0,m}(z)}{\partial z}\right) \middle/ [mk_0(z)A_{0,m}(z)] \right]$$

are slowly varying functions of z. The period of the mth spatial harmonic of the pump magnetic field is a function of z and is

$$l_m(z) = 2\pi \middle/ \left(mk_0(z) + \frac{\partial \varphi_m(z)}{\partial z}\right),$$

where

$$mk_0(z) \gg \left| \frac{\partial \varphi_m(z)}{\partial z} \right|.$$

Similarly, the general form for the scattered electromagnetic field and electrostatic field in terms of the vector potential $\vec{A}(z,t)$ and scalar potential $\phi(z,t)$ is

$$\vec{A}(z,t) = \sum_{n=1} \left[A_{x,n}(z)\cos\left(n \int_0^z k_{x,n}(z')dz' - n\omega t + \theta_{x,n}\right)\hat{e}_x + A_{y,n}(z)\sin\left(n \int_0^z k_{y,n}(z')dz' - n\omega t + \theta_{y,n}\right)\hat{e}_y \right]$$

(A2)

and

$$\phi(z,t) = \sum_{l=1} \phi_l(z)\cos\left(l\int_0^z k_l(z')dz' - l\omega t + \theta_{x,l}\right),$$ (A3)

where the amplitudes of the potentials $A_{x,n}(z)$, $A_{y,n}(z)$, and $\phi_l(z)$, as well as wave numbers $k_{x,n}(z)$, $k_{y,n}(z)$, and $k_l(z)$, are slowly varying functions of z.

Using the same procedure as used to derive Eqs. (7) we obtain the following set of equations for the spatially slowly varying amplitudes and wave numbers:

$$n^2\left(\frac{\omega^2}{c^2} - k_{x,n}^2(z)\right)A_{x,n}(z) = \frac{-4\omega}{c}\int_0^{2\pi/\omega} J_x(z,t)\cos\left(n\int_0^z k_{x,n}(z')dz' - n\omega t + \theta_{x,n}\right)dt_0,$$ (A4a)

$$2nk_{x,n}^{1/2}(z)\frac{\partial}{\partial z}\left(A_{x,n}(z)k_{x,n}^{1/2}(z)\right) = \frac{4\omega}{c}\int_0^{2\pi/\omega} J_x(z,t)\sin\left(n\int_0^z k_{x,n}(z')dz' - n\omega t + \theta_{x,n}\right)dt_0,$$ (A4b)

$$n^2\left(\frac{\omega^2}{c^2} - k_{y,n}^2(z)\right)A_{y,n}(z) = \frac{4\omega}{c}\int_0^{2\pi/\omega} J_y(z,t)\sin\left(n\int_0^z k_{y,n}(z')dz' - n\omega t + \theta_{y,n}\right)dt_0,$$ (A4c)

$$2nk_{y,n}^{1/2}(z)\frac{\partial}{\partial z}\left(A_{y,n}(z)k_{y,n}^{1/2}(z)\right) = \frac{4\omega}{c}\int_0^{2\pi/\omega} J_y(z,t)\cos\left(n\int_0^z k_{y,n}(z')dz' - n\omega t + \theta_{y,n}\right)dt_0,$$ (A4d)

$$l\frac{\partial\phi_l(z)}{\partial z} = 4\int_0^{2\pi/\omega} J_z(z,t)\sin\left(l\int_0^z k_l(z')dz' - l\omega t + \theta_{z,l}\right)dt_0,$$ (A4e)

$$l^2 k_l\phi_l(z) = 4\int_0^{2\pi/\omega} J_z(z,t)\cos\left(l\int_0^z k_l(z')dz' - l\omega t + \theta_{z,l}\right)dt_0.$$ (A4f)

Substituting the expressions for $\vec{J}(z,t)$ from Eq. (13) into Eqs. (A4) and integrating, we obtain

$$n^2\left(\frac{\omega^2}{c^2} - k_{x,n}^2(z)\right)A_{x,n}(z) = 4|e|n_0\frac{\nu_{z0}}{c}\omega\int_0^{2\pi/\omega}\frac{\eta_x(t_0,\tau(t_0,z))}{\eta_z(t_0,\tau(t_0,z))}\cos\left(n\int_0^z k_{x,n}(z')dz' - n\omega\tau(t_0,z) + \theta_{x,n}\right)dt_0,$$ (A5a)

$$2nk_{x,n}^{1/2}(z)\frac{\partial}{\partial z}\left(A_{x,n}(z)k_{x,n}^{1/2}(z)\right) = -4|e|n_0\frac{\nu_{z0}}{c}\omega\int_0^{2\pi/\omega}\frac{\eta_x(t_0,\tau(t_0,z))}{\eta_z(t_0,\tau(t_0,z))}\sin\left(n\int_0^z k_{x,n}(z')dz' - n\omega\tau(t_0,z) + \theta_{x,n}\right)dt_0,$$ (A5b)

$$n^2\left(\frac{\omega^2}{c^2} - k_{y,n}^2(z)\right)A_{y,n}(z) = -4|e|n_0\frac{\nu_{z0}}{c}\omega\int_0^{2\pi/\omega}\frac{\eta_y(t_0,\tau(t_0,z))}{\eta_z(t_0,\tau(t_0,z))}\sin\left(n\int_0^z k_{y,n}(z')dz' - n\omega\tau(t_0,z) + \theta_{y,n}\right)dt_0,$$ (A5c)

$$2nk_{y,n}^{1/2}(z)\frac{\partial}{\partial z}\left(A_{y,n}(z)k_{y,n}^{1/2}(z)\right) = -4|e|n_0\frac{\nu_{z0}}{c}\int_0^{2\pi/\omega}\frac{\eta_y(t_0,\tau(t_0,z))}{\eta_z(t_0,\tau(t_0,z))}\cos\left(n\int_0^z k_{y,n}(z')dz' - n\omega\tau(t_0,z) + \theta_{y,n}\right)dt_0,$$ (A5d)

$$l\frac{\partial\phi_l(z)}{\partial z} = -4|e|n_0\nu_{z0}\int_0^{2\pi/\omega}\sin\left(l\int_0^z k_l(z')dz' - l\omega\tau(t_0,z) + \theta_{z,l}\right)dt_0,$$ (A5e)

$$l^2 k_l\phi_l(z) = -4|e|n_0\nu_{z0}\int_0^{2\pi/\omega}\cos\left(l\int_0^z k_l(z')dz' - l\omega\tau(t_0,z) + \theta_{z,l}\right)dt_0.$$ (A5f)

The expression of the particle orbit equation (14) remains the same. Equations (14), (A5), and along with the definitions of momenta

$$\eta_x(z,\tau) = (|e|/c)[A_{0,x}(z) + A_x(z,\tau)],$$

$$\eta_y(z,\tau) = (|e|/c)[A_{0,y}(z) + A_y(z,\tau)],$$

and

$$\eta_z(z,\tau) = m_0\gamma(z,\tau)V_z(z,\tau),$$ (A6)

form the full set of self-consistent FEL equations.

Setting $n = m = l = 1$, and requiring $k_{x,1}(z) = k_{y,1}(z) = k_s(z)$ and $A_{x,1}(z) = A_{y,1}(z) = A(z)$, equations (A5) reduce to the fundamental harmonic equations in (22) and (23) for a circularly polarized electromagnetic field.

*Present address: Jaycor, Alexandria, Va. 22304.

[1]H. Motz, J. Appl. Phys. 22, 527 (1951).

[2]J. M. J. Madey, J. Appl. Phys. 42, 1906 (1971).

[3]R. B. Palmer, J. Appl. Phys. 43, 3104 (1972).

[4]V. P. Sukhatme and P. W. Wolff, J. Appl. Phys. 44, 2331 (1973).

[5]J. M. J. Madey, H. A. Schwettman, and W. M. Fairbank, IEEE Trans. Nucl. Sci. 20, 980 (1973).

[6]A. T. Lin and J. M. Dawson, Phys. Fluids 18, 201 (1975).

[7]A. Hasegawa, K. Mima, P. Sprangle, H. H. Szu, and V. L. Granatstein, Appl. Phys. Lett. 29, 542 (1976).

[8]F. A. Hopf, P. Meystre, M. O. Scully, and W. H. Louisell, Phys. Rev. Lett. 37, 1342 (1976).

[9]F. A. Hopf, P. Meystre, M. O. Scully, and W. H. Louisell, Opt. Commun. 18, 413 (1976).

[10]W. B. Colson, Phys. Lett. A 59, 187 (1976).

[11]N. M. Kroll and W. A. McMullin, Phys. Rev. A 17, 300 (1978).

[12]P. Sprangle and V. L. Granatstein, Phys. Rev. A 17, 1792 (1978).

[13]S. B. Segall, Report No. KMSF-U860 (1978) (unpublished).

[14]L. R. Elias, Phys. Rev. Lett. 42, 977 (1979).

[15]P. Sprangle and A. T. Drobot, J. Appl. Phys. 50, 2652 (1979).

[16]I. B. Bernstein and J. L. Hirshfield, Phys. Rev. Lett. 40, 761 (1978).

[17]P. Sprangle, R. A. Smith, and V. L. Granatstein, Naval Research Laboratory Memo. Report 3911 (1978). [Also published in Infrared and Millimeter Waves, edited by K. Button (Academic, New York, 1979), Vol. I].

[18]P. Sprangle and R. A. Smith, Phys. Rev. A 21, 293 (1980) (preceding paper).

[19]P. Sprangle and V. L. Granatstein, Appl. Phys. Lett. 25, 377 (1974).

[20]W. M. Manheimer and E. Ott, Phys. Fluids 17, 706 (1974).

[21]V. I. Miroshnichenko, Sov. Tech. Phys. Lett. 1, 453 (1975).

[22]P. Sprangle, V. L. Granatstein, and L. Baker, Phys. Rev. A 12, 1697 (1975).

[23]T. Kwan, J. M. Dawson, and A. T. Lin, Phys. Fluid 20, 581 (1977).

[24]W. Colson and S. Ride (private communication).

[25]V. L. Granatstein and P. Sprangle, IEEE Trans. Microwave Theory Tech. 25, 545 (1977).

[26]A. Hasegawa, Bell Syst. Tech. J. 57, 3069 (1978).

[27]C. W. Planner, Phys. Lett. A 67, 263 (1978).

[28]L. R. Elias, W. M. Fairbank, J. M. J. Madey, H. A. Schwettman, and T. I. Smith, Phys. Rev. Lett. 36, 717 (1976).

[29]D. A. G. Deacon, L. R. Elias, J. M. J. Madey, G. J. Ramian, H. A. Schwettman, and T. I. Smith, Phys. Rev. Lett. 38, 892 (1977).

[30]V. L. Granatstein, M. Herndon, R. K. Parker, and S. P. Schlesinger, IEEE Trans. Microwave Theory Tech. 22, 1000 (1974).

[31]G. Providakes and J. Nation, J. Appl. Phys. 50, 3026 (1979).

[32]V. L. Granatstein, S. P. Schlesinger, M. Herndon, R. K. Parker, and J. A. Pasour, Appl. Phys. Lett. 30, 384 (1977).

[33]D. B. McDermott, T. C. Marshall, S. P. Schlesinger, R. K. Parker, and V. I. Granatstein, Phys. Rev. Lett. 41, 1368 (1978).

[34]R. M. Gilgenbach, T. C. Marshall, and S. P. Schlesinger, Phys. Fluids 22, 971 (1978).

[35]T. C. Marshall, S. Talmadge, and P. Efthimion, Appl. Phys. Lett. 31, 320 (1977).

[36]To our knowledge this technique for enhancing is also being analyzed by N. M. Kroll and M. N. Rosenbluth (private communication).

[37]A. T. Lin and J. M. Dawson, Phys. Rev. Lett. 42, 1670 (1979).